

Geometric and Wave Optic Features in the Optical Transmission Patterns of Injection-molded Mesoscale Pyramid Prism Patterned Plates

Je-Ryung Lee^{1,2}, Tae-Jin Je^{2,3}, Sangwon Woo², Yeong-Eun Yoo^{2,3},
Jun-Ho Jeong^{2,3}, Eun-chae Jeon^{4*}, and Hwi Kim^{1**}

¹Department of Electronics and Information Engineering, Korea University, Sejong 30019, Korea

²Department of Nanomanufacturing Technology, Korea Institute of Machinery and Materials, Daejeon 34103, Korea

³Department of Nanomechatronics, University of Science and Technology, Daejeon 34113, Korea

⁴School of Materials Science and Engineering, University of Ulsan, Ulsan 44610, Korea

(Received November 6, 2017 : revised December 23, 2017 : accepted December 27, 2017)

In this paper, mesoscale optical surface structures are found to possess both geometric and wave optics features. The study reveals that geometric optic analysis cannot correctly predict the experimental results of light transmission or reflection by mesoscale optical structures, and that, for reliable analyses, a hybrid approach incorporating both geometric and wave optic theories should be employed. By analyzing the transmission patterns generated by the mesoscale periodic pyramid prism plates, we show that the wave optic feature is mainly ascribed to the edge diffraction effect and we estimate the relative contributions of the wave optic diffraction effect and the geometric refraction effect to the total scattering field distribution with respect to the relative dimension of the structures.

Keywords : Diffraction, Injection molding, Pyramid prism, Wave optics, Mesoscale structure

OCIS codes : (080.2205) Fabrication, injection molding; (080.2740) Geometric optical design; (050.1950) Diffraction gratings

I. INTRODUCTION

Mesoscale functional optical films or plates with tens (>50 μm) or hundreds (<500 μm) of micro-structures that can be fabricated by mechanical manufacturing method have been actively researched for various applications. For the examples of functional optical sheets such as diffusion sheets, prism sheets, corner-cube sheets, and pyramid sheets, the functional optical elements on the surface of sheets are mesoscale structures and normally fabricated with mechanical machining techniques. Among the mesoscale-structured optical patterns engraved in those films and plates, linear ones such as prism patterns, pyramid patterns or retroreflection patterns, as shown in Fig. 1, are popular structures [1, 2], and are used for improving brightness

performance, LED radiation, chromatic aberrations, and the polarization extinction ratio. Normally, the main processes of their design, analysis, and assessment are based on the theory of geometric optics. In industrial settings, in order to create high-quality mesoscale structured optical patterns, the methods for design, analysis, and assessment using geometrical optics simulation programs are normally used [3]. However this approach often leads to the goods produced proving less efficient than was expected during the design, analysis and modeling of the patterns and can give rise to unexpected problems. This is because something unexplainable from the perspective of geometrical optics occurs as patterns becomes smaller. In addition, it is highly likely that errors are created while working the metal molds and producing the optical films or plates

*The authors contributed equally to this work.

†Corresponding authors: *jeonec@ulsan.ac.kr, ORCID 0000-0002-6951-219X

**hwikim@korea.ac.kr, ORCID 0000-0002-4283-8982

Color versions of one or more of the figures in this paper are available online.



This is an Open Access article distributed under the terms of the Creative Commons Attribution Non-Commercial License (<http://creativecommons.org/licenses/by-nc/4.0/>) which permits unrestricted non-commercial use, distribution, and reproduction in any medium, provided the original work is properly cited.

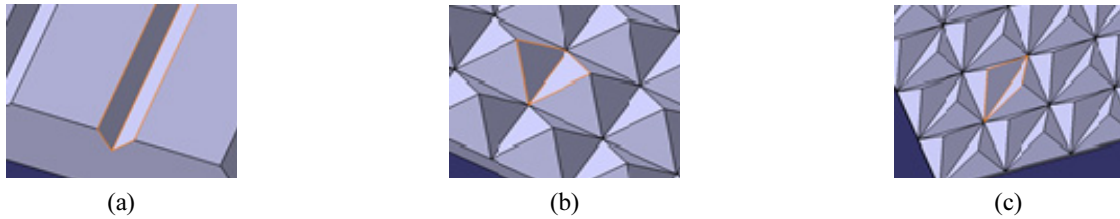


FIG. 1. Mesoscale optical structures; (a) prism pattern, (b) pyramid pattern, and (c) retroreflection pattern.

cause the optical films or plates to create different optical patterns from those originally intended. Despite these problems only few studies on the design of mesoscale optical products have considered such errors. In this paper, the light transmission properties of a mesoscale periodic pyramid structure with a $50\ \mu\text{m}$ pitch size is studied to determine the role of geometric and wave optic features in mesoscale optical structures. Both geometric analysis and wave-optic analysis are used in a hybrid approach. In order to prepare polymeric pyramid plate samples, we machined metal molds and used injection molding to produce polymeric pyramid plates. The optical properties of the resulting polymeric pyramid plates were then both evaluated experimentally and analyzed quantitatively through numerical simulation. In addition, 3D modeling of the mesoscale-structured optical patterns with errors was conducted to analyze the refractive effects of the polymeric pyramid patterned plates by geometrical optics simulation. Not only geometrical optics but also wave optics should be taken into consideration, when analyzing the experimentally observed field distribution formed by patterns of particularly small dimension and analyzing and evaluating the quality of those mesoscale-structured optical patterns. Due to this, we also assessed optical properties based on wave optics so as to analyze the optical properties of polymeric pyramid plates with mesoscale-structured optical patterns. Additionally, this paper looks at the relative contributions of geometrical and wave optics to the optical pattern as the size of optical patterns changes. In Section 2, the experimental observation of the light transmission pattern of a mesoscale polymer pyramid plane is presented. In Section 3, a geometric optic simulation analysis of the target sample is shown and its limitations are discussed. In Section 4, a wave optic simulation analysis is carried out and compared with the geometric-only simulation results. The relative contributions of the geometric optic and wave optic effects to the total scattering field distribution are analyzed, and the concluding remarks follow.

II. EXPERIMENTAL OBSERVATION OF LIGHT TRANSMISSION PATTERNS OF MESOSCALE POLYMER PYRAMID PLATES

In order to determine what optical effects the mesoscale-patterned polymeric pyramid plates with mesoscale patterns

have, we observed the image on the rear-screen onto which the transmitted light is shed when a $532\ \text{nm}$ He-Ne laser beam was vertically incident on the back side of the sample. The experiment was conducted after setting the distances between the laser, the polymeric pyramid plate, and the screen as depicted in Fig. 2. The simulation modeling was based on the same arrangement. For the experiment, mesoscale optical pattern molds were produced and from them, optical plates were created through an injection molding process. To compare a partially unmolded optical plate and an optimally formed optical plate, two optical plates were produced under different injection temperatures. The polymeric pyramid plate was designed and fabricated by us. We produced a metal mold for injection molding of polymeric pyramid plates with mesoscale-structured optical patterns as optimized in the previous study [4]. The intended pattern, a mesoscale-structured optical pattern optimized to improve optical efficiency, was a periodically repeated pyramid with $25\ \mu\text{m}$ height, $50\ \mu\text{m}$ pitch, and 90° apex angle as shown in Fig. 3(b). The patterns were made with a $90\ \text{mm} \times 60\ \text{mm}$ nickel mold using an ultrafine planer. UVM-450 (Toshiba) was used for the process at a $200\ \text{mm/s}$ processing speed. We used the 90 degree diamond tool and adopted an overlap processing method [5] so as to make the processed surface of better quality. The SEM image of Fig. 3(b) revealed a surface relief of square pyramidal patterns. There was no burr, and the four base lines and the vertices of the square pyramidal pattern were very sharp. However, the vertex at the top of the pyramid was not a perfect dot, but a line about $1.7\ \mu\text{m}$ long. In order to translate the less-processed part into length, we calculated the height of an isosceles triangle with a $1.7\ \mu\text{m}$ base line and obtained a height

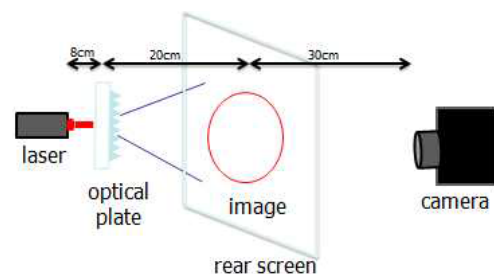


FIG. 2. Optical pattern generated by mesoscale-pyramid patterns under the normal incident illumination of a $532\ \text{nm}$ HeNe laser.

value of about $0.85 \mu\text{m}$. The square pyramidal pattern relief machined in nickel was around $24.1 \mu\text{m}$ deep. We used transparent PMMA (Poly methyl methacrylate), which is widely used in injection molding with metal molds featuring machined patterns, and produced polymeric pyramid plates with mesoscale-structured optical patterns. In the experiment, we used, an SE-50D, an injection molder made by Sumitomo and produced a PMMA plate with 40 mm width, 70 mm length, and 2 mm thickness. Because it is difficult to shape the vertices of the square pyramid by injection molding, we optimized the injection direction and speed, and the temperature of the metal mold according to an existing study [6]. Since we did injection molding after producing metal molds with relief pyramidal patterns, the patterns were injected as intaglio. Although the boundaries between the pyramids that were formed in the direction parallel to the injection direction, were molded as lines even in low temperatures, those in the direction perpendicular to the injection direction were molded convexly. We attribute this incomplete molding to consolidation made from the surface while the metal mold was filled by resin during fine pattern molding, rapidly undermining fluidity and creating weld lines on the pattern boundaries [7]. To avoid such artifacts we optimized the molding conditions by using an 80°C mold temperature and a 150 mm/s injection speed.

The optical transmission image in Fig. 3(a) shows two straight lines forming the shape of a cross horizontally and vertically with four linking rhombus-shaped curved lines. This optical transmission pattern image is formed by the

optical plate shown in Fig. 3(b), which was produced under the optimal molding conditions mentioned above featuring an 80°C mold temperature and 150 mm/s injection speed. The optimized injection-molded plate showed line-shaped boundaries in directions parallel and perpendicular to the injected direction. However, the microscope showed that this shape does not have perfect pyramidal edges but that the edges have a certain thickness as shown in Fig. 3(c). The thickness was $4.65 \mu\text{m}$ on the side perpendicular to the injected direction and $3.49 \mu\text{m}$ on the side parallel to it. Measuring the size of intaglio pyramid formed by the plate produced as above, we found the width was $50 \mu\text{m}$, the same as the processed metal mold. However the height, which was measured through a 3D microscope, was $22 \mu\text{m}$ as shown in Fig. 3(d). After comparing the heights in the perpendicular and parallel directions to the injection with a 3D microscope, we discovered that the two heights differ only slightly. The part shot by the laser got significantly brighter, which we thought was due to the round edges and the vertices of the injected pyramid consisting of curved surfaces rather than points.

Next, we compare the polymeric pyramid plates produced by these different molds. After measuring the edges of the polymeric pyramid plate which was injection-molded in Fig. 3(c) above, we found that the polymeric pyramid plate injected at 80°C has edges in the vertical and horizontal directions which differ only slightly from each other. For the polymeric pyramid plate injected at 60°C , however, the edges in the vertical direction were 2.67 times thicker than those in the horizontal direction as shown in Fig. 4(c).

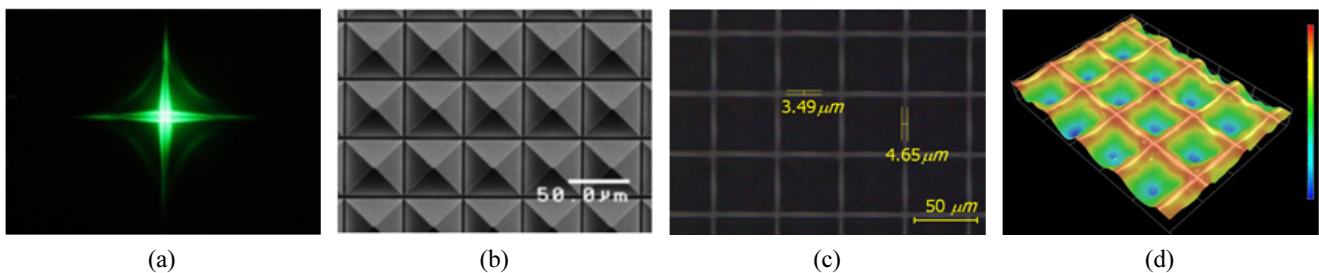


FIG. 3. Optical plane of the molding produced under optimal conditions; (a) light pattern, (b) 2D SEM image of metallic mold, (c) 2D microscope image of the polymeric pyramid pattern, and (d) 3D profile of the pyramid pattern measured by 3D optical microscope.

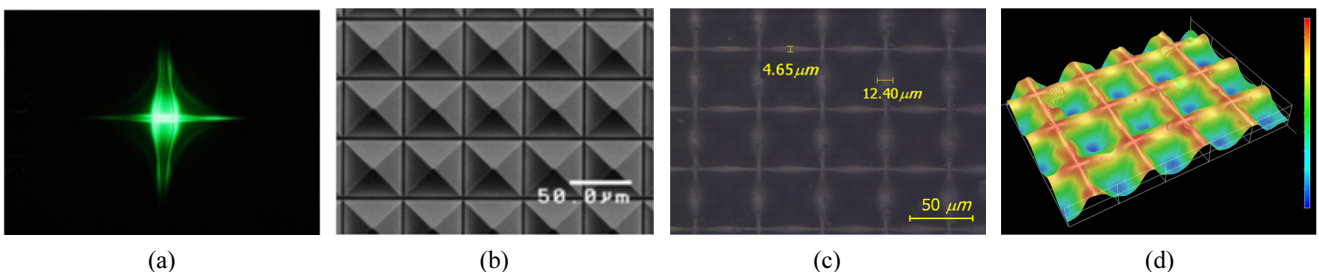


FIG. 4. Optical plane of the molding produced under non-optimum conditions; (a) light pattern, (b) 2D SEM image of metallic mold, (c) 2D microscope image of the polymeric pyramid pattern, and (d) 3D profile of the pyramid pattern measured by 3D optical microscope.

The polymeric pyramid plate made of the same mold can show structural errors according to the conditions of injection molding, which, in turn, have an influence on optical field. The differences in the molded polymeric plates are reflected in the light patterns they produce in the optical experiment. The resulting width of the vertical lines in the light pattern shown in Fig. 4(a) with the sub-optimal molding is 3.18 times thicker than that of Fig. 3(a) with the optimal molding. It is inferred that the light spread out much more due to the refraction effect at the rounding edges. It is found that the polymeric pyramid plate injected at 60°C formed convex patterns between each pyramid in the horizontal direction as a result of the way the intaglio pyramid was injected.

III. GEOMETRIC-OPTIC ANALYSIS

In order to check the results of the optical experiment presented in Section 2, which were found to vary from plate to plate, we conducted a geometric optic simulation used in industrial settings. We molded polymeric pyramid plates injected by CATIA and performed a ray-tracing simulation using ZEMAX. The resulting modeled polymeric pyramid plates are shown in Figs. 5(a) and 5(b). The scaled numerical model shown in Fig. 5(a) is of the polymeric pyramid plates injected at 80°C, and that in Fig. 5(b) is of the one injected at 60°C with the same specifications. The ZEMAX simulation results for the two samples are presented in Figs. 5(c) and 5(d), respectively, showing only the refraction effects. In the simulation results, neither the cruciform lines nor the rhombus lines are observed, but the four points of light refracted by the four inclined facets of the pyramid plate and a horizontally stretched bright spot in the central region are. In Fig. 5(d), a stretching of the light is also evident in the optical experiment and the spreading width of the central spot was measured as 3.18 times longer than its length. As when measuring the width and length in the results obtained from the ZEMAX simulation, we found that the width is 3.27 times longer than the length, which agrees well with the experimental results. As shown in Figs. 3(a) and 4(a), the vertical line of the latter stretches more than that of

the former, which is ascribed to refraction effects caused by the bottom pyramid pattern facing blunt edges that were yet to be injected.

Since the geometric optic simulation only models the refraction effect, it does not reproduce the cruciform and rhombus lines apparent in the experimental light pattern as they which formed by edge diffraction. The vertical line shown in Fig. 4(a) stretches more than that shown in Fig. 3(a). This is ascribed to the blunt edges that were not precisely injected.

The spreading of the vertical line observed in the optical experiment is interpreted by the refraction of diffracted light, and does not appear in ZEMAX simulation results shown in Fig. 5 because the simulation does not model diffraction by edges. From the simulation result, one can infer that the light in the middle spreads in a horizontal direction but the vertical line in the cross shape does not. In the further simulations, the extent of unmolding was varied when conducting the simulation and this allowed the correlation between the unmolded portion of the PMMA plate and the horizontal spread of light to be measured. The result showed that the extent of unmolding and the area across which the light spread are proportionate.

IV. WAVE OPTICAL ANALYSIS

An optics simulation was also conducted to observe the effects induced by the diffraction of light on the mesoscale-optical patterns that were unable to be observed using commercial ray-tracing programs. In order to explain the diffraction effect, we develop a mathematical model of non-paraxial diffraction field of the polymer pyramid plate. For this, the angular spectrum formulas of diffractive wave [8, 9] were used and a wave optics simulator allowing the assignment of the mesoscale-pyramid pattern's length, width, and height was implemented. A plane wave is incident on the flat bottom interface of the grating substrate and the transmitted plane wave is refracted by the Snell's law on the top interface of the structure. The unit pyramid intaglio consists of four triangle facets. In a previous study, the mathematical model of an illuminating triangle facet in 3D free space was introduced for a computer generated

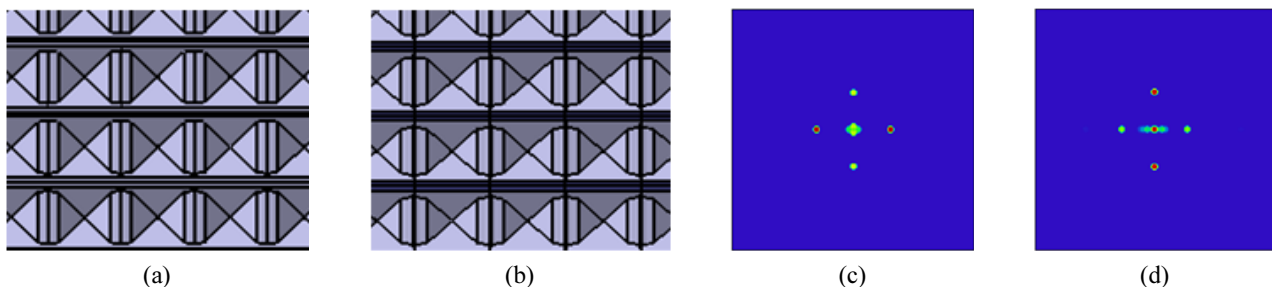


FIG. 5. Modeling of (a) the polymeric pyramid plate injected at 80°C and (b) the polymeric pyramid plate injected at 60°C. The ZEMAX optical simulation result of (c) the optical plate injected at 80°C and (d) the one injected at 60°C.

hologram of arbitrary polygon objects [10] and this theory is employed in our analysis. The illuminating triangle facet is modeled by a titled triangular aperture and the carrier wave which passes through it. The light field distribution of the illuminating triangle facet is given by the angular spectrum representation,

$$W_k(x, y, z) = \int_{-\infty}^{\infty} \int_{-\infty}^{\infty} A_k(\alpha, \beta) e^{j2\pi(\alpha x + \beta y + \gamma z)} d\alpha d\beta \quad (1)$$

where the angular spectrum of the light field $A_k(\alpha, \beta)$ is given in Eq. (10) of ref. [10]. Let us apply the mesh model to explain the light transmission of the pyramid plate.

In the wave optical simulation, the laser beam is incident upon the four sides and edges of the rectangular pyramid; the beam incident upon the sides is then refracted while those refracted upon the edges are diffracted. The laser beam refracted through the pyramid's four sides is separated into four beams of different directions. Assume the pyramid plate is periodic and infinitely repeated on the x-y plane, and then the propagating plane wave will meet two interfaces which are the boundaries between free space and the PMMA. The first interface is an infinite flat bottom surface. All we need to calculate is the wave vector of a plane wave in the PMMA medium. Let us assume $\eta_0 \exp(j2\pi(\alpha_l x + \beta_l y + \gamma_l z))$ is an incident plane wave to the bottom interface of the structure. The spatial frequency α_l, β_l and γ_l has a relation expressed by $\gamma_l = \sqrt{(n_f / \lambda)^2 - \alpha_l^2 - \beta_l^2}$, where n_f is the refractive index of free space and λ is the wavelength of the incident wave. According to Snell's law, the tangential components of the wave vector are invariant regardless of the medium. Thus, $\alpha_{II} = \alpha_l, \beta_{II} = \beta_l$ is valid, where α_{II} and β_{II} are spatial frequencies of transmitted field in the PMMA, and γ_{II} is $\sqrt{(n_p / \lambda)^2 - \alpha_{II}^2 - \beta_{II}^2}$. The second interface consists of the tilted triangular surfaces of the pyramid structure. The diffraction field of the pyramid structure is analyzed by the linear coherent superposition of the partial diffraction on each triangular surface. In the local coordinate system (x', y', z') of a triangle facet, the triangle facet should be

placed on the $x'y'$ plane. Let $2\pi(\alpha'_{II}, \beta'_{II})$ be the tangential component of the wave vector in the local coordinate system. Then these tangential components will not vary outside of the triangle facet as $(\alpha'_{III}, \beta'_{III}) = (\alpha'_{II}, \beta'_{II})$, and γ'_{III} is equal to $\sqrt{(n_f / \lambda)^2 - \alpha'_{III}{}^2 - \beta'_{III}{}^2}$. The spatial frequency (α, β, γ) in the global coordinate system is obtained by the relation between local coordinate and global coordinate.

$$\begin{pmatrix} \alpha \\ \beta \\ \gamma \end{pmatrix} = \begin{pmatrix} \cos \theta \cos \phi & -\sin \phi & \sin \theta \cos \phi \\ \cos \theta \sin \phi & \cos \phi & \sin \theta \sin \phi \\ -\sin \theta & 0 & \cos \theta \end{pmatrix} \begin{pmatrix} \alpha'_{III} \\ \beta'_{III} \\ \gamma'_{III} \end{pmatrix} \quad (2)$$

Where θ and ϕ are the longitudinal tilt angle and azimuthal angle of the normal vector of the triangular facet [10]. Finally, the angular spectrum expression of the diffraction field propagating from the PMMA pyramid structure to the free space is represented by substituting (α, β, γ) of Eq. (2) into Eq. (1). This analytic model can explain the non-paraxial light field of structures with great depth or steep surfaces including their related refraction and total reflection phenomena, except for those cases that include multiple internal reflections.

In the optic simulation, the pyramid's top and each corner has the form of a dot and a straight line, respectively, as shown in Fig. 6(a). Analyzing the designed mesoscale-optical pattern by the wave optics simulation results in total internal reflection and only the light that penetrates the edge of the mesoscale-optical pattern (that is the edge of the pyramid) is visible. However, the height of the pyramid pattern produced through the injection molding process into the metal model was 22 μm , but because the experiment used a lower height it resulted in both geometrical optics and diffractive optics as shown in Fig. 6(b). Figure 6(b) illustrates a cross shape composed of two straight lines—one vertical and one horizontal—and a rhombus shape composed of four curved lines. The four spots in Fig. 6(b) are the optical pattern induced by the refraction. The four rhombus-shaped curved lines are the diffraction pattern generated by the sharp line-edges of the pyramid pattern that, as discussed in the paper, cannot be simulated by only the geometric optic analysis. The edges of the rhombus are curved rather than straight because the edges of the pyramid are spatially tilted from the horizontal plane. The edges are not spatially parallel to the sides upon which the beam is incident, so the light penetrating the edges creates a diffractive pattern with a curved shape known as a conical diffraction [10, 12]. The conical diffraction is observable with bare eyes when at the point where the height of the pyramid reached 11 μm , as it is increased in 1 μm increments from 0 μm . As previously described, this effect results when the edges are not spatially parallel with the sides of incidence; it seems

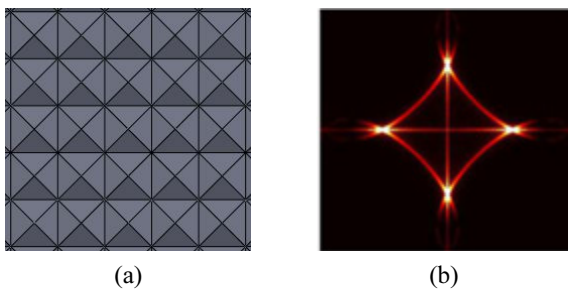


FIG. 6. (a) Pyramid structure used and (b) resulting light pattern simulated by the wave optic model.

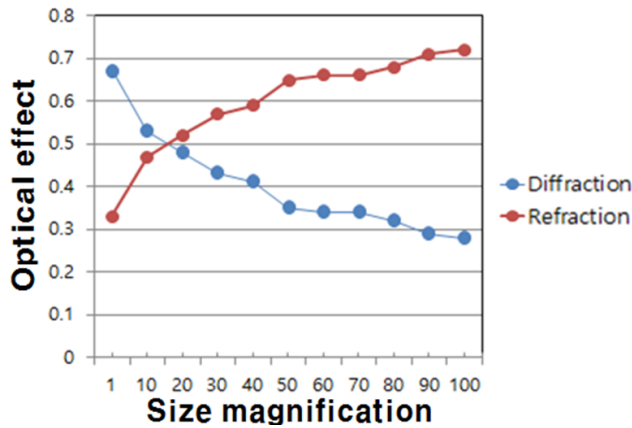


FIG. 7. Changes in the contributing portion of the geometric optics and wave optics on the light transmission pattern with pyramid pattern size change.

that to be able to observe the phenomenon with bare eyes, the minimum pyramid height required is 11 μm . The vertical and horizontal straight lines are also diffractive effects resulting from the checkerboard shape of the bottom side of the rectangular pyramid.

Lastly, the wave optic analysis examined the refraction and diffraction effects resulting from changes in the ideal rectangular pyramid pattern's size. The geometric effect is estimated by the light power of the geometric pattern measured in the localized area of the four spots refracted by the four inclined facets of the pyramid structure. The diffraction effect is estimated by the light power of the diffraction pattern except the geometric light pattern induced by the sharp edges. The diffraction optical effect in Fig. 7 is estimated by the total power allotted to the whole set of rhombus-shaped curved and cross-shaped lines. This experiment studied the refraction and diffraction effects when the size of the pyramid was enlarged up to 100 times its original size (length 5,000 μm , height 2,200 μm , respectively) while keeping the ratios constant. As illustrated in Fig. 7, the diffraction effect becomes more vivid when the structure size becomes smaller, but the refraction effect becomes dominant with increase of the structure size. For the enlargement of 20 times the original size (length 1,000 μm and height 440 μm respectively) or over, the refraction effect was higher than the diffraction effect. Thus, as the size of the rectangular pyramid becomes measurable in mm, the diffraction effect decreases. In electromagnetic theory, the asymptotic hybrid methods using wave features in terms of geometric optics have been developed [13-18]. However, those methods are limited to use with perfect conducting objects not widely used for optical structures. It should be researched to build up the optical hybrid analysis framework for mesoscale structures.

V. CONCLUSION

In this study, an optic plate was designed that possesses a certain structured mesoscale-optical pattern and the resulting optical transmission patterns were analyzed based on geometrical optics and wave optics. The numerical simulation has shown that the relative changes in the refraction and diffraction effects are dependent on the scale of the pyramid element. By showing the diffraction effect generated by mesoscale optical structures and explaining how pattern size or molding artifacts can affect optical qualities associated with diffraction effect, this study can be useful for many optical engineering endeavors related to design of mesoscale optical structures. Further research will focus on improving the simulation tool, which employs hybridization of geometric optics and wave optics simulation techniques for more general mesoscale optical elements.

ACKNOWLEDGMENT

This work was partly supported by the Industrial Strategic Technology Development Program (10052641) funded by the Ministry of Trade, Industry & Energy (MI, Korea) and partly by the 'Development of Convergence Manufacturing Technology for Functional Nanostructures of Active Devices' by the 'National Research Council of Science & Technology'.

REFERENCES

1. H. R. Saghai, A. Asgari, H. B. A. Nejad, and A. Rostami, "A study in optical properties of AlGaIn/GaN pyramid and prism-shape quantum dots," *Physica E* **41**, 245-253 (2008).
2. M. Karl, D. Rülke, T. Beck, D. Z. Hu, D. M. Schaadt, H. Kalt, and M. Hetterich, "Reversed pyramids as novel optical micro-cavities," *Superlattices Microstruct.* **47**, 83-86 (2010).
3. E.-c. Jeon, T.-J. Je, E.-S. Lee, E.-S. Park, J.-R. Lee, H. Choi, S. Chang, and S.-K. Choi, "Optimization of hybrid LED package system for energy saving based on micro machining technology and Taguchi method," *Int. J. Precis. Eng. Manuf.* **14**, 1113-1116 (2013).
4. E.-c. Jeon, J.-H. Jeon, T.-J. Je, S. Chang, D.-S. Choi, and S.-K. Choi, "Development of hybrid LED package system having micro optical pattern based on micro machining technology and Taguchi method," *MNE* **37**, 475-476 (2011).
5. T.-J. Je, E.-c. Jeon, S.-C. Park, D.-S. Choi, K.-H. Whang, and M.-C. Kang, "Improvement of machining quality of copper-plated roll mold by controlling temperature variation," *Trans. Nonferrous Met. Soc. China* **21**, 37-41 (2011).
6. S.-W. Woo, E.-c. Jeon, K.-M. Lee, Y.-E. Yoo, and T.-J. Je, "Study on injection molding of micro pattern diffusion plate for LED lighting," *J. Korean Soc. Precis. Eng.* **10**, 271 (2012).
7. E.-c. Jeon, J.-R. Lee, S.-W. Woo, E.-S. Park, H. Kim, T.-J. Je, Y.-E. Yoo, and K.-H. Whang, "Manufacturing of micro-pyramid patterns and verification of their optical effects," *Int. Conf. Micromanuf.* **14**, 467-472 (2013).
8. H. Kim, Y. J. Lim, B. Yang, K. Choi, and B. Lee, "Geometrical analysis of optical transmission characteristics of prism sheet layers," *Opt. Eng.* **44**, 128001-1-11 (2005).

9. H. Kim and B. Lee, "Geometric optics analysis on light transmission and reflection characteristics of metallic prism sheets," *Opt. Eng.* **25**, 084004-1-10 (2006).
10. H. Kim, J. Hahn, and B. Lee, "Mathematical modeling of the triangle-mesh-modeled three-dimensional surface objects for digital holography," *Appl. Opt.* **47**, 117-127 (2008).
11. R. A. Watts, J. R. Sambles, and J. B. Harris, "An experimental test of conical diffraction theory," *Opt. Commun.* **135**, 189-192 (1997).
12. L. I. Goray and G. Schmidt, "Solving conical diffraction grating problems with integral equations," *J. Opt. Soc. Am. A* **27**, 585-597 (2010).
13. J. B. Keller, "Geometrical theory of diffraction," *J. Opt. Soc. Am.* **52**, 116-130 (1962).
14. R. G. Kouyoumjian and P. H. Pathak, "A uniform geometric theory of diffraction for an edge in a perfectly conducting surface," *Proc. IEEE* **62**, 1448-1461 (1974).
15. D. P. Bouche, F. A. Molinet, and R. Mittra, "Asymptotic and hybrid techniques for electromagnetic scattering," *Proc. IEEE* **81**, 1658-1684 (1993).
16. M. A. Alonso, "Wigner functions in optics: describing beams as ray bundles and pulses as particle ensembles," *Adv. Opt. Photon.* **3**, 272-365 (2011).
17. D. Dragoman, "The Wigner distribution function in optics and optoelectronics," *Prog. Opt.* **37**, 1-56 (1997).
18. F. F. Jobsis, "Noninvasive, infrared monitoring of cerebral and myocardial oxygen sufficiency and circulatory parameters," *Sci.* **198**, 1264-1267 (1977).